Available online at www.sciencedirect.com
ScienceDirect
Journal of Molecular Catalysis A: Chemical 259 (2006) 91–98
JOURNAL OF MOLECULAR CATALYSIS A: CHEMICAL
www.elsevier.com/locate/molcata

Reduced forms of Rh(III) containing MCM-41 silicas as hydrogenation catalysts for arene derivatives

Maya Boutros [a], Franck Launay [a,*], Audrey Nowicki [b], Thomas Onfroy [a], Virginie Herledan-Semmer [a], Alain Roucoux [b], Antoine Gédéon [a,*]

[a] *Université Pierre et Marie Curie, UMR CNRS 7142, Laboratoire Systèmes Interfaciaux à l'Echelle Nanométrique, Case 196, 4 place Jussieu, Paris F-75252 Cedex 05, France*
[b] *Equipe Synthèse Organique et Systèmes Organisés, UMR CNRS 6226 "Sciences Chimiques de Rennes", Ecole Nationale Supérieure de Chimie de Rennes, Avenue du Gal Leclerc, Rennes F-35700, France*

Received 2 April 2006; received in revised form 31 May 2006; accepted 1 June 2006
Available online 20 July 2006

Abstract

Rhodium containing mesoporous siliceous materials with MCM-41 pore architecture have been prepared via a template directed hydrolysis-polycondensation of tetraethoxysilane and rhodium(III) chloride in aqueous ammonia. The effect of aging and hydrothermal conditions on rhodium incorporation and on the porous structure of the resulting solids has been examined using elemental analysis, powder X-ray diffraction (XRD), N_2 sorption measurements and transmission electron microscopy (TEM). Optimized synthetic conditions afforded MCM-41 materials with Si/Rh 1400 and 120. Subsequent reduction of rhodium oxides species by hydrogen emphasized that the growth of Rh^0 particles (2–3 nm) is controlled by the porosity of the support. The conditions and efficiency of this step were evaluated through H_2-TPR (temperature programmed reduction) and IR monitored CO adsorption studies. The resulting materials showed a good catalytic activity and stability in the hydrogenation of arene derivatives under mild pressure and temperature. *Cis*/*trans* selectivity of dimethylcyclohexanes was discussed in the light of dispersion measurements.

Keywords: Hydrogenation; CO adsorption; MCM-41; Rhodium(0) nanoparticles; Arene derivatives

1. Introduction

Silica or aluminosilica materials with an hexagonal structured mesopore network like MCM-41 or SBA-15 have been extensively studied since the first reports dealing with their synthesis [1,2]. Their high specific surface area, porous volume and adjustable pore size diameter make them ideal supports for the preparation of highly dispersed heterogeneous catalysts [3,4]. To meet this goal, various heteroelements and mainly metals have been introduced in order to get active materials in acid [5], oxidation [5,6] or hydrogenation reactions [5]. Zero-valent metals including rhodium are usually incorporated via salt precursors which are reduced in situ. Particle growth during the reduction process is thus expected to be limited due to the confinement of the metal inside the mesopore channels [7]. Synthetic pathways involving mesoporous silica or aluminosilica described up to now are mainly based on impregnation processes [8–11] or ion exchanges between rhodium(III) species and protons [10,12,13]. Grafting of Rh complexes through organic linkers [14–20] has also been investigated. However, less studies are concerned by the addition of rhodium salts into the synthesis gel of mesoporous solids [21–23] or xerogels [24,25]. Rh heterogeneous catalysts are usually tested either in gas/solid or liquid/solid hydrogenation [13–16,18,21,22], hydroformylation [17,18,26] reactions or in pollutants removal [10,12].

In this work, we describe the incorporation of Rh(III) into a siliceous MCM-41 via a sol–gel pathway in aqueous ammonia and the reduction of the resulting Rh oxides into Rh(0) particles. The active phase will be characterized by IR monitored CO adsorption and hydrogenation tests performed under mild conditions. The present study takes part to our effort to develop simple inorganic heterogeneous Rh(0) catalysts for liquid phase hydrogenation of arene derivatives [27,28]. Such solids could be used

* Corresponding authors. Tel.: +33 1 44 27 71 43.
E-mail addresses: franck.launay@upmc.fr (F. Launay), Antoine.gedeon@upmc.fr (A. Gédéon).

1381-1169/$ – see front matter © 2006 Elsevier B.V. All rights reserved.
doi:10.1016/j.molcata.2006.06.007

for the reduction of aromatic content in oils [21,22] as well as for the conversion of phenol into a cyclohexanol/cyclohexanone mixture which is the starting material for adipic acid synthesis [29]. Furthermore, partial incorporation of the particles in the walls of the mesopores could lead to a better anchorage of the catalyst and induce unusual selectivities.

2. Experimental

2.1. Materials

RhO_x-MCM41 materials, denoted RhO_x-M, were prepared by modifying the method described for pure silica MCM-41 reported by Brühwiler and Frei [30]. The chemicals used were: cetyltrimethylammonium bromide (CTAB, Aldrich), tetraethoxysilane (TEOS, Fluka), aqueous ammonia (30 wt.% NH_3, Carlo/Erba) and rhodium chloride hydrate ($RhCl_3{\cdot}xH_2O$, % Rh = 40.79, $x = 2.25$, Strem chemicals).

CTAB (2.2 g) was dissolved under slight warming (308 K) in a mixture of 52 mL of distilled H_2O and 24 mL of aqueous ammonia. Rhodium chloride hydrate was introduced into the solution which was stirred for 15 min until it became clear. Then, 10 mL of TEOS were slowly added. The resulting gel composition was $1SiO_2$:0.13CTAB:yRh:8.4NH_3:83H_2O. The gel was aged for $t_a = 3$ h (or 24 h) at room temperature, then transferred into a Teflon® bottle and was hydrothermally treated at $T_h = 383$ K (or 423 K) for $t_h = 48$ h (or 96 h). The solid product was filtered, washed with distilled water, dried at 333 K for 24 h and calcined in air, first at 573 K for 2 h then at 823 K for 12 h (heating rate was 2 K min^{-1}).

The desired catalysts Rh^0-MCM41, denoted Rh^0-M, were prepared by the reduction of the calcined solid RhO_x-M in the presence of H_2. In a typical experiment, the sample was pre-heated under vacuum from 298 to 573 K (ramping rate: 60 K h^{-1}). After cooling, H_2 gas (flow 8.3 mL min^{-1}) was passed through the sample while heating from 298 to 493 K (ramping rate: 12 K h^{-1}). The temperature was maintained at 493 K for 1 h and hydrogen gas was then evacuated. Finally, the sample was further heated from 493 to 673 K (ramping rate: 60 K h^{-1}) and kept at 673 K for 12 h before cooling to room temperature under vacuum.

2.2. Characterization

2.2.1. X-ray diffraction

The calcined or reduced samples were evaluated by powder X-ray diffraction using a Bruker D8 Advance X-ray diffractometer at Cu Kα radiation (λ = 0.15418 nm). PXRD measurements were performed from 1° to 7° (2θ) in steps of 0.02° with a count time of 6 s at each point.

2.2.2. Nitrogen sorption

The specific surface area, pore volume and pore diameter of all calcined or reduced samples were determined from N_2 sorption data obtained at 77 K using an ASAP 2010 micromeritics instrument. Prior to the analysis, the samples were outgassed at 473 K until a stable static vacuum of 2×10^{-3} Torr was reached. The pore diameter and specific pore volume were calculated according to the Barrett–Joyner–Halenda (BJH) model. The specific surface area was obtained with the Brunauer–Emmett–Teller (BET) equation.

2.2.3. Chemical analysis

Silicon and rhodium compositions of the various materials were determined by ICPAES in the CNRS center at Vernaison (France).

2.2.4. Transmission electron microscopy (TEM)

Transmission electron analyses were performed using a JEOL TEM 100CXY electron microscope. The powdered samples were dispersed in ethanol and the resulting suspensions deposited on a copper grid coated with a porous carbon film.

2.2.5. Temperature-programmed reduction (TPR) measurements

TPR studies were carried out with a TPD/R/O instrument (ThermoQuest) which consists of a cylindrical quartz microreactor, a vertical furnace and a gas chromatograph equipped with a thermal conductivity detector (TCD). A typical experiment was conducted using 50 mg of RhO_x-M. First, the reactor was purged by passing He gas (10 mL min^{-1}) through the sample at 323 K for 30 min. The treatment of the solid was carried out in an oxygen gas flow (10 mL min^{-1}) by heating the sample from 323 to 973 K (ramping rate: 20 K min^{-1}), and keeping the final temperature at 973 K for 1 h. The reactor was cooled to 323 K before analysis. The thermoreduction process was performed by passing a 5% H_2/Ar gas mixture (20 mL min^{-1}) through the sample while heating from 323 to 773 K (ramping rate: 5 K min^{-1}). The final temperature was kept at 773 K for 30 min.

2.2.6. Infrared spectroscopy

IR spectra were recorded on a Nicolet Magna 550 FT-IR spectrometer (resolution: 4 cm^{-1}, 128 scans). Samples were pressed into pellets (ca. 20 mg for 2 cm^2) and activated at 423 K. The solids were first heated under vacuum at 423 K (30 min). This step was followed by a treatment in H_2 ($P_{equilibrium}$ = 13.3 kPa, 30 min) and an evacuation (30 min) at 423 K before cooling down to room temperature (RT). CO was introduced at RT and IR spectra were recorded at different equilibrium pressures (from 26.6 Pa to 4.0 kPa). In the ν(CO) region (2200–1750 cm^{-1}), spectra were obtained by subtracting the spectra of activated catalysts from those after CO adsorption.

The amount of CO involved in each of the observed species, namely $Rh^I(CO)_2$ cations (gem-dicarbonyls), linearly and bridged bonded CO on Rh^0, was calculated from Eq. (1):

$$n_{CO,X} = \frac{A_X S}{\varepsilon_{CO,X} m} \quad (1)$$

where $n_{CO,X}$ (μmol g^{-1}) stands for the number of CO involved in the species X, A_X the integrated absorbance (cm^{-1}) of the bands attributed to the species X, S the surface of the pellet (cm^2), $\varepsilon_{CO,X}$ the integrated molar absorption coefficient of CO (cm μmol^{-1}) for the species X and m is the weight (g) of the pellet. In order to

evaluate the integrated absorbance of the bands characteristic of the three CO adsorption states, spectra were curve-fitted keeping the FWHM and the position of a given peak essentially constant. Best fits were generally obtained with Gaussian peaks. The use of a Lorentzian profile did not significantly affect the quantitative results. The different molar absorption coefficients (cm μmol^{-1}) were previously determined by Rasband and Hecker [31]:

$\varepsilon_{(CO,linear)} = 13 \pm 2\,cm\,\mu mol^{-1}$;

$\varepsilon_{(CO,bridged)} = 42 \pm 6\,cm\,\mu mol^{-1}$;

$\varepsilon_{(CO,gem)} = 130 \pm 50\,cm\,\mu mol^{-1}$

Based on the amount of CO adsorbed, the number of accessible Rh atoms (n_{Rh}) was calculated using Eq. (2):

$$n_{Rh} = n_{CO,linear} + 2n_{CO,bridged} + \frac{n_{CO,gem}}{2} \quad (2)$$

This value was used to determine the dispersion percentage (D) and the average particles size (l). The latter was calculated assuming cubic shapes where only five of the six faces of the cube are exposed to the gas phase.

2.2.7. Catalytic tests

Rh^0-M samples were used as catalysts in the hydrogenation of different arene derivatives (styrene, *o*-, *m*- and *p*-xylene, phenol) at room temperature using two sets of hydrogen pressure (0.1 and 1 MPa). Whatever the conditions, the catalyst (50 or 100 mg) was dispersed in hexane (10 mL) under magnetic stirring during 15 min prior to the introduction of the substrate (100 equiv. $metal^{-1}$). Products were quantified with *n*-decane as internal standard using a Delsi Nermag gas chromatograph equipped with a SPB™-5 capillary column and a FID detector. Recycling of the catalysts was tested by the renewal of the substrate once it is consumed.

3. Results and discussion

Rhodium supported catalysts are very attractive for many reactions as the production of adipic acid or the removal of pollutants [10,12]. Many Rh-mesoporous systems have been described up to now [8–13,21–23] but the combination of the use of $RhCl_3$ salt in aqueous ammonia with the subsequent reduction of Rh oxide as well as their use in the hydrogenation of arene derivatives under mild conditions have not been explored. The procedure retained was motivated by the fact that, unlike aqueous Rh species, ammine Rh(III) complexes [32,33] are not reducible at 383 K by the ethanol [34,35] formed during the hydrolysis and condensation of TEOS.

All samples described in this work were obtained by a procedure adapted from the preparation of Si-MCM41 according to Brühwiler et al. [30]. The optimization of the synthesis conditions has been achieved by varying the hydrothermal time and temperature, as well as the aging time.

3.1. Characterization of the support and active phase

The reference synthesis involves an aging time of 3 h and a 48 h-hydrothermal treatment at 383 K. Table 1 shows that, for a molar ratio Si/Rh = 80 in the reaction mixture, the obtained value can vary in the range of 85–165 depending on the synthesis parameters.

Sample RhO_x-M(I) obtained under Brühwiler's conditions is characterized by slightly lower surface area and pore volume than for pure Si-MCM41. The final Si/Rh value of the solid is 120. Indeed, the insertion of Rh(III) in the silica framework is difficult due to size considerations (ionic radii of Rh^{3+} and Si^{4+} are 66.5 and 40 pm, respectively). The analysis of all the results shows that the insertion of Rh(III) cation in the MCM-41 material is facilitated by reducing the aging (t_a) and hydrothermal (t_h) times, and increasing the hydrothermal treatment temperature T_h (Table 1). However, at $T_h = 423$ K (RhO_x-M(IV)), one can observe a significant decrease in surface area and pore volume. It can also be noticed that partial reduction of rhodium(III) is observed during the 423 K hydrothermal treatment.

Nitrogen sorption isotherms of Si-MCM41 and RhO_x-M(I, II and III) samples are characterized by a quite sharp inflection at $P/P_0 = 0.2$–0.35 (Fig. 1). As a result, the corresponding materials can be considered as MCM-41 solids. On the other hand, the high incorporation of Rh in RhO_x-M(IV) has led to the collapse of the mesopore structure. Moreover, the isotherms of all RhO_x-M samples as well as those of the parent one present a large type H4-hysteresis loop at P/P_0 between 0.5 and 1.0. This could indicate the existence of some structural void defects [36,37]. According to Lin et al. [36], the size and shape of these voids are mainly affected by the Si/heteroelement ratio and the water content in the synthetic gel. It can be noticed that RhO_x-M(I) is characterized by the smallest H4-hysteresis loop.

Powder XRD patterns of RhO_x-M(I–III) samples show the strong reflection typical for the (1 0 0) plane of MCM-41 (Fig. 2). Secondary peaks are also well-resolved indicating long range ordering of the hexagonal mesopore structure. RhO_x-M(IV) is definitely not a structured mesoporous material.

Table 1
Influence of the synthesis parameters on the composition and textural data of RhO_x-M (Si/Rh = 80 in the initial reaction mixture)

Sample	Aging time, t_a (h)	Hydrothermal conditions		Rh (wt.%)	Si/Rh (mol/mol)	Surface area ($m^2\,g^{-1}$)	Pore volume ($cm^3\,g^{-1}$)	Pore diameter (nm)
		t_h (h)	T_h (K)					
Si-MCM41	3	48	383	–	–	800	0.70	2.6
RhO_x-M(I)	3	48	383	1.30	120	720	0.64	2.8
RhO_x-M(II)	24	48	383	1.05	150	640	0.62	3.1
RhO_x-M(III)	3	96	383	0.95	165	600	0.51	2.9
RhO_x-M(IV)	3	48	423	1.80	85	260	0.17	5.2

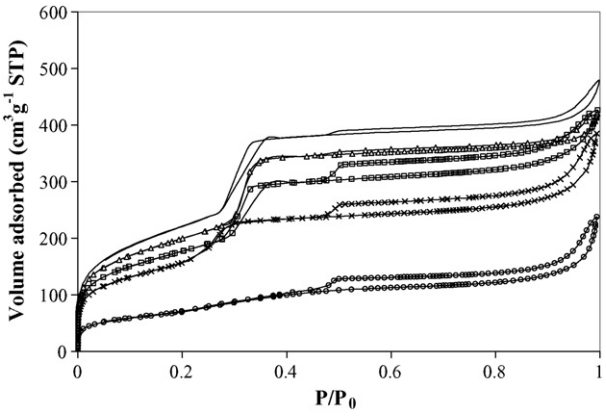

Fig. 1. Nitrogen adsorption/desorption isotherms of silica MCM-41 and RhO_x-M(I–IV) samples (Si/Rh = 80 in the initial reaction mixture): (−) Si-MCM41, (△) RhO_x-M(I), (□) RhO_x-M(II), (×) RhO_x-M(III), and (◯) RhO_x-M(IV).

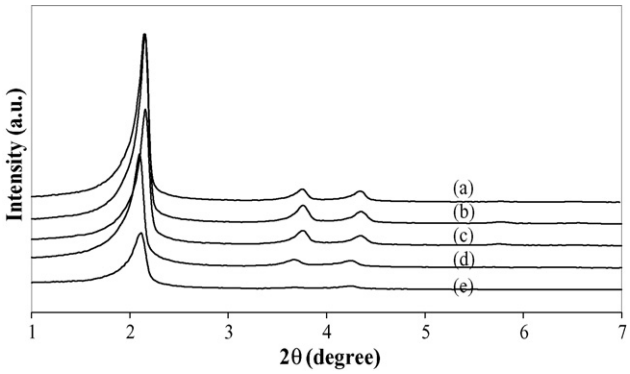

Fig. 3. Small angle X-ray diffraction patterns of silica MCM-41 and RhO_x-M(I) samples *vs*. Rh loading: (a) Si-MCM41, (b) RhO_x-M(I)/1400, (c) RhO_x-M(I)/330, (d) RhO_x-M(I)/120, and (e) RhO_x-M(I)/70.

As a result of the preliminary study, synthetic conditions of sample RhO_x-M(I) were retained and the validity of the "one-pot" procedure was further investigated by expanding the range of Si/Rh ratio. New samples (RhO_x-M(I)/experimental Si/Rh ratio), were thus obtained with Si/Rh values between 70 and 1400. Whatever the amount of rhodium introduced, XRD patterns are typical of hexagonal MCM-41 (Fig. 3). As expected, increasing amounts of Rh lead to the gradual decrease of the intensities of each peak. Indeed, the reflections corresponding to the (1 1 0) and (2 0 0) planes cannot be easily discerned for RhO_x-M(I)/70 indicating that it is much less structured than other samples.

Nitrogen adsorption–desorption isotherms of the different solids are still characteristic of MCM-41 with more or less structural defects (Fig. 4). As long as the effective rhodium content is low (Si/Rh > 120), i.e. RhO_x-M(I)/1400 and RhO_x-M(I)/330 samples, it appears that the textural parameters are similar (±5%) to those of the pure silica material Si-MCM41 (Table 2). More significant changes (−10 to −25%) are observed for RhO_x-M(I)/120 and RhO_x-M(I)/70. The decrease of the BET surface area and pore volume is the result of the perturbations of the self-assembly of surfactant aggregates due to the incorporation of bigger amounts of metal during the co-condensation process. Whatever the sample, the mean porous diameter does not seem to change significantly.

Air-calcined rhodium containing RhO_x-M(I) solids have been converted at 493 K (see Section 2.1) to Rh^0-M(I) using H_2 as a reducing agent. The treatment conditions used have been established in accordance with the results of temperature programmed reduction studies (Fig. 5). The different solids are reduced at a temperature lower than 450 K. Excepted for RhO_x-M(I)/1400, the reduction profiles are characterized by a main peak at 370 K and a minor one at 416 K, respectively. Given that Rh(III) species are relatively easier reduced compared to lower oxidation states, the first peak might be attributed to Rh_2O_3. As a consequence, the second one might be assigned to Rh_2O and RhO [38]. The occurrence of two signals can also be interpreted by differences in the location and/or in the sizes of Rh_2O_3 particles [23].

Nitrogen sorption data of Rh^0-M(I) and RhO_x-M(I) indicate that the reduction process does not affect strongly the textural parameters of the solids (data not shown). The intensities of XRD reflections are also comparable but the diffraction peaks of the reduced samples are shifted to lower angles. For example, values of the hexagonal parameter, a_0, of Rh^0-M(I)/120 and RhO_x-M(I)/120 are 4.95 and 4.7 nm, respectively. This implies that

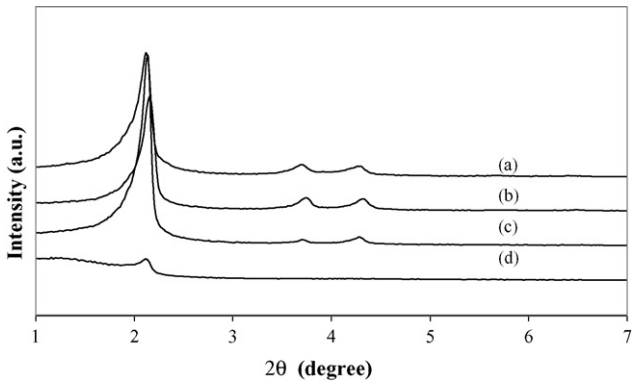

Fig. 2. Small angle X-ray diffraction patterns of RhO_x-M(I–IV) samples (Si/Rh = 80 in the initial reaction mixture): (a) RhO_x-M(I), (b) RhO_x-M(II), (c) RhO_x-M(III), and (d) RhO_x-M(IV).

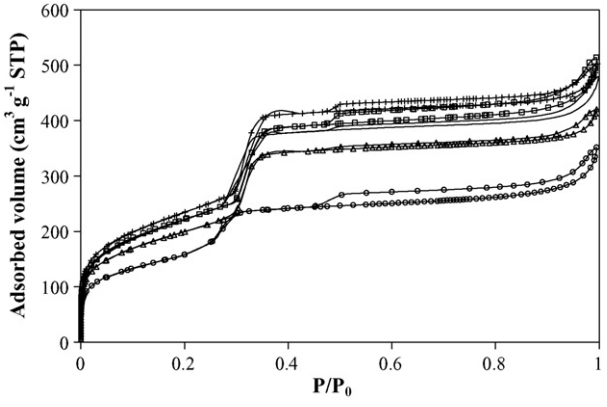

Fig. 4. Nitrogen adsorption/desorption isotherms of silica MCM-41 and RhO_x-M(I) samples *vs.* Rh loading: (−) Si-MCM41, (|) RhO_x-M(I)/1400, (□) RhO_x-M(I)/330, (△) RhO_x-M(I)/120, and (◯) RhO_x-M(I)/70.

Table 2
Influence of the Si/Rh initial ratio on the composition and textural data of RhO_x-M(I) samples

Sample	Si/Rh (M)	Rh (wt.%)	Surface area ($m^2\ g^{-1}$)	Pore volume ($cm^3\ g^{-1}$)	Pore diameter (nm)
Si-MCM41	–	–	800	0.70	2.6
RhO_x-M(I)/1400	1400	0.10	850	0.75	2.9
RhO_x-M(I)/330	330	0.50	800	0.68	2.7
RhO_x-M(I)/120	120	1.30	720	0.64	2.8
RhO_x-M(I)/70	70	2.05	600	0.48	2.7

the wall thickness of MCM-41 increases during the reduction step.

TEM images of Rh^0-M(I)/120, Rh^0_x-M(I)/330 and Rh^0_x-M(I)/1400 (Fig. 6) indicate that channels are still structured. Dispersed particles of rhodium(0) are observed inside the pores of Rh^0-M(I)/120 and Rh^0_x-M(I)/330. Their average size (2–3 nm) is very close to the pore diameter of MCM-41, thus evidencing the influence of the support in the control of particles growth. TEM analysis of Rh^0-M(I)/1400 revealed fewer particles with a 4 nm-mean diameter.

Carbon monoxide adsorption followed by infrared spectroscopy is a powerful tool for the characterization of supported metal particles [39]. Indeed this technique provides information about the oxidation degree of rhodium [40]. The higher the metal oxidation state, the higher the frequency of adsorbed CO. Quantitative treatment of the adsorption data leads also to the evaluation of the number of metal atoms which are accessible to the gas [31] and hence to the determination of the metal dispersion and the average size of the particles.

The IR spectra of CO adsorbed on the samples Rh^0-M(I)/120, Rh^0_y-M(I)/330 and Rh^0_y-M(I)/1400 under an equilibrium CO pressure of 1.33 kPa exhibit three main bands situated at 2092, 2070, 2040 cm^{-1} and a broader one around 1960–1800 cm^{-1}. According to the literature, the band at 2070 cm^{-1} could be attributed to CO linearly bonded to Rh^0 atoms [40,41]. Evolution of the broad band with increasing amounts of CO (spectra not shown) suggests the presence of two components centred at 1915 and 1880 cm^{-1} (Fig. 7). These latter have been attributed to bridged CO adsorbed on different crystallographic plans of Rh particles [42]. Bands at 2092 and 2040 cm^{-1} can be assigned to symmetric and anti-symmetric stretching vibration modes of

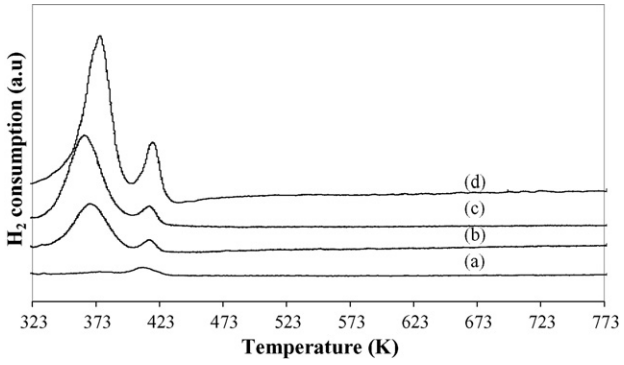

Fig. 5. H_2-TPR profiles of RhO_x-M(I) samples: (a) RhO_x-M(I)/1400, (b) RhO_x-M(I)/330, (c) RhO_x-M(I)/120, and (d) RhO_x-M(I)/70.

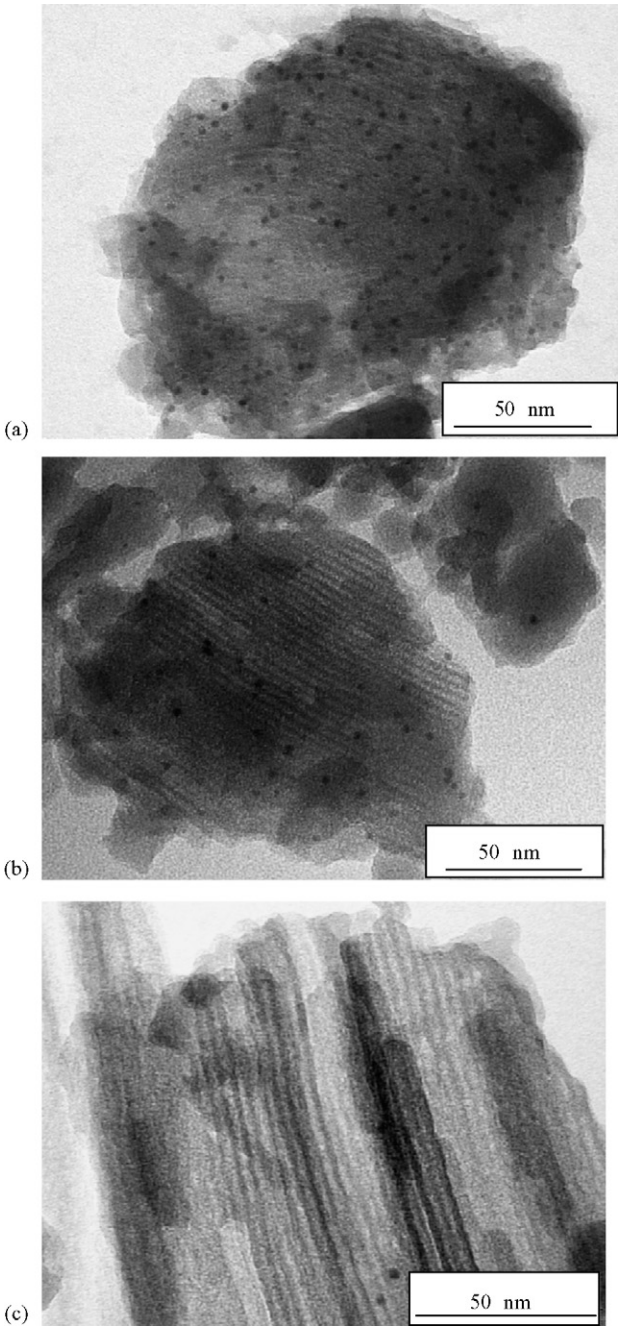

Fig. 6. Transmission electron micrographs of (a) Rh^0-M(I)/120, (b) Rh^0-M(I)/330, and (c) Rh^0-M(I)/1400 samples.

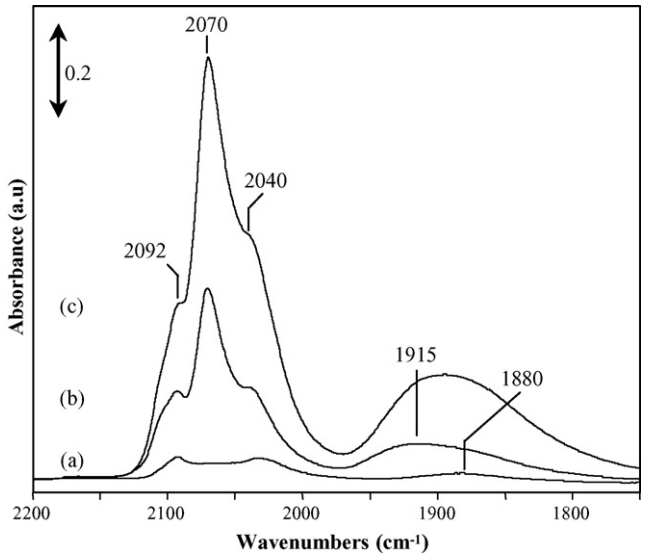

Fig. 7. IR spectra of CO adsorbed onto Rh^0-M(I) samples: (a) Rh^0-M(I)/1400, (b) Rh^0-M(I)/330, and (c) Rh^0-M(I)/120. (Spectra measured and normalized to 100 mg of powder under a CO equilibrium pressure of 1.33 kPa.)

gem-dicarbonyl species (i.e. $Rh^I(CO)_2$), respectively [40]. The absence of bands at higher frequencies (>2092 cm^{-1}) proves that Rh^0-M(I) samples do not contain Rh^{2+} or Rh^{3+} ions.

The evolution of the amount of CO involved in each of the three adsorption states (linear, bridged and gem) (Fig. 8) shows that the number of all rhodium species progressively increases as a function of the Rh loading. According to these results, most of the CO are bonded to Rh^0. The weak proportion of Rh^I species indicates that reduction of Rh^{x+} to zero-valent Rh is complete at 423 K under H_2.

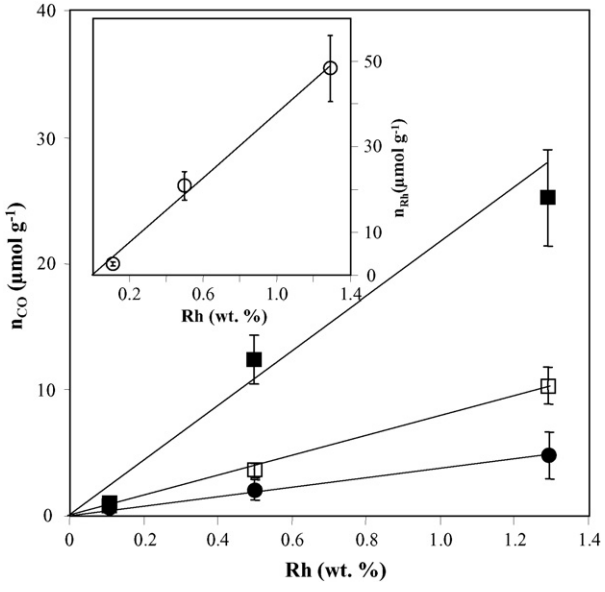

Fig. 8. Evolution of the amount of CO (n_{CO}) involved in linear (■), bridged (□), gem (●) adsorption states *vs.* Rh loading. Inset: Total number of Rh atoms (n_{Rh}) accessible to CO molecules (○) *vs.* Rh loading. (Error bars are linked to the accuracy of the $\varepsilon_{CO,X}$ values.)

Table 3
Amount of accessible Rh atoms (n_{Rh}), dispersion percentage (D) and average particles size (l) of the Rh^0-M(I) samples

Sample	Rh (wt.%)	n_{Rh} (µmol g^{-1})	D[a] (%)	l[b] (nm)
Rh^0-M(I)/1400	0.10	2.6 ± 0.5	24.4 ± 4.2	3.9 ± 0.7
Rh^0-M(I)/330	0.50	20.7 ± 3.3	42.6 ± 6.9	2.3 ± 0.4
Rh^0-M(I)/120	1.30	48.2 ± 7.7	38.5 ± 6.2	2.5 ± 0.4

[a] $D = (n_{Rh}/n_{Rh\ total}) \times 100$.
[b] $l = 5[m_{Rh}/(n_{Rh} Na \rho_{Rh} \sigma_{Rh})]$, where m_{Rh}: Rh weight per gram of catalyst (g); Na: Avogadro's number; ρ_{Rh}: Rh density (1.24×10^{-20} g nm^{-3}); σ_{Rh}: surface occupied by one Rh atom (0.072 nm^2).

The quasi-linear increase of the number of Rh atoms accessible to CO *versus* Rh loading suggests a similar Rh dispersion on all samples (Fig. 8 inset). Indeed, dispersion values for Rh^0-M(I)/120 and Rh^0-M(I)/330 are close to 40% which is in good accordance with values for other silica supports [43]. The Rh dispersion mesurement in Rh^0-M(I)/1400 is less accurate due to the weak absorption bands of CO. Its low value could be associated to the aggregation of particles during the reduction treatment (Table 3). The average particle sizes calculated from CO adsorption, assuming cubic shapes, are in good agreement with those determined from TEM images. According to IR and TEM results, it can be deduced that all the Rh is incorporated in relatively small particles exposed to the gas phase. Thus, the presence of Rh embedded in the wall of the mesoporous silica and then inaccessible to the probe molecules can be ruled out.

3.2. Catalytic performances of the materials

Catalytic hydrogenation of different arene derivatives (styrene, xylenes and phenol) has been performed with Rh^0-M(I) solids in hexane at room temperature. The tests were carried out either under 0.1 or 1 MPa H_2 (Table 4). Complete hydrogenation of the aromatic rings occurred in all the conditions. Quasi-quantitative (90–100%) yields of products have been obtained under atmospheric hydrogen pressure within 24 h whereas a complete conversion has been reached in all cases under 1 MPa in less than 3 h. Results are similar for Rh^0-M(I)/330 and Rh^0-M(I)/120, the two catalysts being tested with substrate/Rh = 100. The catalysts could be reused for a second run without loss of activity. In the case of styrene, hydrogenation of the vinyl substituent occurred before that of the phenyl ring. Products with partially hydrogenated benzenic rings could not be detected excepted for the test with phenol. In this last case, the completion of the reaction (i.e. 100% cyclohexanol) under 1 MPa was obtained after 2.8 h. The detailed kinetic profile (not shown here) indicates that the intermediate, cyclohexanone (2 mol of H_2 consumed per mole of phenol), can be obtained in significant amounts. Its yield rises up to 45% at 0.5 h. As a result the cyclohexanone/cyclohexanol ratio is close to 50/50 before 0.5 h and slowly decreases to 0/100.

Hydrogenation of disubstituted benzene derivatives such as xylenes is very informative. Whatever the xylene isomer considered, the selective formation of the thermodynamically less favourable *cis* dimethylcyclohexanes products is observed. Hydrogenation of the more symmetrical isomer, *p*-xylene, turns

Table 4
Hydrogenation of typical arene derivatives

Substrate	Catalyst	Products	*Cis*/*trans* selectivity (%)	P_{H_2} (MPa)	Reaction time (h)	Yield (%)
Styrene	Rh^0-M(I)/330	Ethylcyclohexane	–	0.1	24	92
	Rh^0-M(I)/330		–	1	1.2	100 (100)[a]
	Rh^0-M(I)/120		–	0.1	24	94
m-Xylene	Rh^0-M(I)/330	1,3-Dimethylcyclohexane	76/24	0.1	24	100
	Rh^0-M(I)/330		81/19	1	0.7	100 (100)[a]
	Rh^0-M(I)/120		76/24	0.1	24	100
	Rh^0-M(I)/120		80/20	1	0.5	100 (100)[a]
o-Xylene	Rh^0-M(I)/330	1,2-Dimethylcyclohexane	89/11	1	0.75	100 (100)[a]
p-Xylene	Rh^0-M(I)/330	1,4-Dimethylcyclohexane	72/28	1	0.75	100 (100)[a]
Phenol	Rh^0-M(I)/330	Cyclohexanol Cyclohexanone	–	1	0.5 (2.8)	55 (100)[b] 45 (0)[b]

Catalyst (50 mg and 100 mg at $P = 0.1$ and 1 MPa, respectively), substrate/Rh = 100 (molar ratio), hexane (10 mL), temperature (293 K).
[a] Yield of the second run after a new loading in substrate.
[b] Yields of products after 2.8 h.

out to be the less selective transformation in agreement with the results of other catalytic systems [44,45]. Selective formation of *cis* products is also reported by literature data on rhodium-catalyzed hydrogenation reactions performed with homogeneous [46], biphasic [44,46,47], gas/solid [48,49] and liquid/solid [50,51] catalytic systems. Formation of the *cis* isomer is generally interpreted as the addition of six hydrogen atoms from the metal surface to the aromatic ring. *Trans* compounds, commonly observed as minor products, are related to the outcome of the partially hydrogenated intermediates. Precisely, they are formed when a dimethylcyclohexene derivative dissociates from the catalyst surface and then re-associates with the opposite "face" before further hydrogenation. Whatever the isomer of xylene considered, it can be noticed that the values of *cis*/*trans* ratio are higher than unity and increase with hydrogen pressure. This suggests that *trans* products are formed through the "roll-over" mechanism. Dimethylcyclohexenes would isomerize on the surface, roll over and be hydrogenated to give *trans* derivatives. Such reaction scheme is in agreement with the absence of dimethylcyclohexenes in the liquid phase [48]. It is interesting to note that similar *cis*/*trans* ratio of 1,3-dimethylcyclohexane were obtained for Rh^0-M(I)/120 and Rh^0-M(I)/330. These results, which need further confirmation, could be associated with their similar values of Rh dispersions (40%) (vide supra). Indeed, various studies dealing with the gas-phase hydrogenation of xylene showed that metal dispersion could influence the *cis*/*trans* dimethylcyclohexane ratio [48,49,52].

4. Conclusion

The present work reports on the synthesis of MCM-41 type mesoporous solids by the co-condensation of rhodium(III) chloride and tetraethoxysilane in aqueous ammonia. Preliminary studies were performed to optimize the synthesis conditions (aging time, hydrothermal time and temperature) in order to get a good compromise between the mesopore structuration and rhodium contents of the resulting solids. RhO_x-M(I) materials with a MCM-41 type structure and an effective Si/Rh molar ratio between 120 and 1400 have thus been obtained.

The procedure used allowed the synthesis of RhO_x-M(I) and the corresponding Rh^0-M(I) samples in two distinct steps. Similarities between the mesopore diameters and the rhodium particle sizes are compatible with the control of the particle growth by the silica support. The efficiency of Rh(III) reduction and the size of the nanoparticles are confirmed by IR monitored CO adsorption data. Rh^0-M(I) materials with metal dispersion value of 40% turned out to be interesting heterogeneous catalysts for the hydrogenation of different arene derivatives at room temperature under mild hydrogen pressures. Complete hydrogenation of the aromatic rings occurred in all the conditions. Xylene isomers are mainly converted to *cis* dimethylcyclohexanes with values of the *cis* selectivity between 70 and 90%. Rhodium (0) particles formed inside MCM-41 materials lead to an efficient and reusable catalytic system. Further studies are in progress in order to precise the role of the metal environment on the selectivity.

Acknowledgements

FT-IR measurements were performed in the Laboratory "Catalyse et Spectrochimies, UMR 6506, CNRS-ENSICAEN". We also gratefully acknowledge Prof. Jean-Luc Bonardet for his experimental assistance in the TPR analysis of our materials.

References

[1] J.S. Beck, J.C. Vartuli, W.J. Roth, M.E. Leonowicz, C.T. Kresge, K.D. Schmitt, C.T.-W. Chu, D.H. Olson, E.W. Sheppard, S.B. McCullen, J.B. Higgins, J.L. Schlenker, J. Am. Chem. Soc. 114 (1992) 10834.
[2] D. Zhao, J. Feng, Q. Huo, N. Melosh, G.H. Fredrickson, B.F. Chmelka, G.D. Stucky, Science 279 (1998) 548.
[3] A. Wingen, F. Kleitz, F. Schüth, Springer Ser. Chem. Phys. 75 (2004) 283.
[4] D.E. De Vos, M. Dams, B.F. Sels, P.A. Jacobs, Chem. Rev. 102 (2002) 3615.
[5] B. Viswanathan, B. Jacob, Catal. Rev. 47 (2005) 1.
[6] M. Ziolek, Catal. Today 90 (2004) 145.
[7] A. Taguchi, F. Schüth, Microp. Mesop. Mater. 77 (2005) 1.
[8] J. Jamis, J.R. Anderson, R.S. Dickson, E.M. Campi, W.R. Jackson, J. Organomet. Chem. 603 (2000) 80.

[9] M. Pillinger, C.D. Nunes, P.D. Vaz, A.A. Valente, I.S. Goncalves, P.J.A. Ribeiro-Claro, J. Rocha, L.D. Carlos, F.E. Kühn, Phys. Chem. Chem. Phys. 4 (2002) 3098.
[10] X. Xu, H. Xu, F. Kapteijn, J.A. Moulijn, Appl. Catal. B 53 (2004) 265.
[11] P.L. Dhepe, A. Fukuoka, M. Ichikawa, Phys. Chem. Chem. Phys. 5 (2003) 5565.
[12] R.Q. Long, R.T. Yang, J. Phys. Chem. B 103 (1999) 2232.
[13] A. Crosman, W.F. Hoelderich, J. Catal. 232 (2005) 43.
[14] C. Gonzalez-Arellano, A. Corma, M. Iglesias, F. Sanchez, Inorg. Chim. Acta 357 (2004) 3071.
[15] C.M. Crudden, D. Allen, M.D. Mikoluk, J. Sun, Chem. Commun. (2001) 1154.
[16] F. Goettmann, D. Grosso, F. Mercier, F. Mathey, C. Sanchez, Chem. Commun. (2004) 1240.
[17] J.P.K. Reynhardt, Y. Yang, A. Sayari, H. Alper, Chem. Mater. 16 (2004) 4095.
[18] C.M. Standfest-Hauser, T. Lummerstorfer, R. Schmid, H. Hoffmann, K. Kirchner, M. Puchberger, A.M. Trzeciak, E. Mieczyńska, W. Tylus, J.J. Ziólkowski, J. Mol. Catal. A: Chem. 210 (2004) 179.
[19] A.M. Liu, K. Hidajat, S. Kawi, J. Mol. Catal. A: Chem. 168 (2001) 303.
[20] V. Dufaud, F. Beauchesne, L. Bonneviot, Angew. Chem. Int. Ed. 44 (2005) 3475.
[21] S. Albertazzi, R. Ganzerla, C. Gobbi, M. Lenarda, M. Mandreoli, E. Salatelli, P. Savini, L. Storaro, A. Vaccari, J. Mol. Catal. A: Chem. 200 (2003) 261.
[22] M. Jacquin, D.J. Jones, J. Roziere, S. Albertazzi, A. Vaccari, M. Lenarda, L. Storaro, R. Ganzerla, Appl. Catal. A: Gen. 251 (2003) 131.
[23] R.S. Mulukutla, T. Shido, K. Asakura, T. Kogure, Y. Iwasawa, Appl. Catal. A 228 (2002) 305.
[24] C.K. Lambert, R.D. Gonzalez, J. Solid State Chem. 158 (2001) 154.
[25] P. Reyes, G. Pecchi, J.L.G. Fierro, Langmuir 17 (2001) 522.
[26] T.E. Bitterwolf, J.D. Newell, C.T. Carver, R.S. Addleman, J.C. Linehan, G. Fryxell, Inorg. Chim. Acta 357 (2004) 3001.
[27] R. Mouawia, M. Boutros, F. Launay, V. Semmer-Herlédan, A. Gédéon, V. Mévellec, A. Roucoux, Stud. Surf. Sci. Catal. 158 (2005) 1573.
[28] V. Mevellec, PhD Thesis, Université Rennes I, 2005.
[29] C. Thurman, in: M. Grayson, D. Eckroth (Eds.), Kirk-Othmer Encycl. Chem. Technol., Wiley, New York, 1982, p. 373.
[30] D. Brühwiler, H. Frei, J. Phys. Chem. B 107 (2003) 8547.
[31] P.B. Rasband, W.C. Hecker, J. Catal. 139 (1993) 551.
[32] M. Hancock, B. Nielsen, J. Springborg, Inorg. Synth. 24 (1986) 220.
[33] J.A. Osborn, K. Thomas, G. Wilkinson, Inorg. Synth. 13 (1971) 213.
[34] N. Toshima, K. Hirakawa, Polym. J. 31 (1999) 1127.
[35] A. Roucoux, J. Schulz, H. Patin, Chem. Rev. 102 (2002) 3757.
[36] H.P. Lin, S.T. Wong, C.Y. Mou, C.Y. Tang, J. Phys. Chem. B 104 (2000) 8967.
[37] S.T. Wong, H.P. Lin, C.Y. Mou, Appl. Catal. A: Gen. 198 (2000) 103.
[38] T. Wu, Q. Yan, F. Mao, Z. Niu, Q. Zhang, Z. Li, H. Wan, Catal. Today 93–95 (2004) 121.
[39] K. Hadjiivanov, G.N. Vayssilov, Adv. Catal. 47 (2002) 307.
[40] C.A. Rice, S.D. Worley, C.W. Curtis, J.A. Guin, A.R. Tarrer, J. Chem. Phys. 74 (1981) 6487.
[41] A.C. Yang, C.W. Garland, J. Phys. Chem. 61 (1957) 1504.
[42] J.C. Lavalley, J. Saussey, J. Lamotte, R. Breault, J.P. Hindermann, A. Kiennemann, J. Phys. Chem. 94 (1990) 5941.
[43] T. Beutel, O.S. Alekseev, Y.A. Ryndin, V.A. Likholobov, H. Knözinger, J. Catal. 169 (1997) 132.
[44] A. Roucoux, J. Schulz, H. Patin, Adv. Synth. Catal. 345 (2003) 222.
[45] V. Mévellec, A. Roucoux, E. Ramirez, K. Phillipot, B. Chaudret, Adv. Synth. Catal. 346 (2004) 72.
[46] G.S. Fonseca, A.P. Umpierre, P.F.P. Fichtner, S.R. Teixeira, J. Dupont, Chem. Eur. J. 9 (2003) 3263.
[47] R.J. Bonilla, B.R. James, P.G. Jessop, Chem. Commun. (2000) 941.
[48] A.K. Neyestanaki, P. Mäki-Arvela, H. Backman, H. Karhu, T. Salmi, J. Väyrynen, D.Y. Murzin, J. Catal. 218 (2003) 267.
[49] R. Gomez, G. Del Angel, V. Bertin, React. Kinet. Catal. Lett. 44 (1991) 517.
[50] C.W. Chen, L. Zhang, S.J. Su, M.Y. Huang, S.F. Mao, Y.Y. Jiang, Polym. Adv. Technol. 7 (1996) 711.
[51] C.W. Chen, H. Yu, M.Y. Huang, Y.Y. Jiang, Polym. Adv. Technol. 7 (1996) 79.
[52] M. Viniegra, G. Córdoba, R. Gómez, J. Mol. Catal. 58 (1990) 107.